THE ROLE OF BOUNDARY LAYER AEROSOL PARTICLES FOR THE DEVELOPMENT OF DEEP CONVECTIVE CLOUDS: A HIGH-RESOLUTION 3D MODEL WITH DETAILED (BIN) MICROPHYSICS APPLIED TO CRYSTAL-FACE

Delphine Leroy, Wolfram Wobrock and Andrea I. Flossmann

Laboratoire de Météorologie Physique, Université Blaise Pascal-CNRS-OPGC,
24, avenue des Landais, F-63177 Aubière Cedex, France
E-mail : A.Flossmann@opgc.univ-bpclermont.fr

1. ABSTRACT

The presented study reproduces aircraft microphysical measurements using a three-dimensional (3D) model with detailed microphysics and is then used to analyze in particular the role of boundary layer aerosol particles on the anvil and the ice phase. The simulated case is a convective cloud which develops a large anvil around 10 km height and which was sampled during the Cirrus Regional Study of Tropical Anvils and Cirrus Layers – Florida Area Cirrus Experiment (CRYSTAL-FACE). The model couples the 3D dynamics of a cloud scale model with a detailed mixed phase microphysical code. The microphysical package considers the evolution of the wet aerosol particles, drop and ice crystals spectra on size grids with 39 bins. With this model hereafter called DESCAM 3D, we are able to simulate the cloud with features close to the observed and to provide explanations of the observed phenomena concerning cloud microphysics as well as cloud dynamics.

The same CRYSTAL-FACE cloud has already been simulated by other groups also with a 3D model with detailed microphysics. They investigated the role of mid-tropospheric aerosol particles versus boundary layer aerosol on the microphysical properties of the anvil. Similar simulations with our DESCAM 3D lead to quite different results. Reducing the number of mid-tropospheric aerosol particles causes only minor changes in the cloud anvil. However, changing the aerosol particle spectrum in the boundary layer from clean to polluted modifies strongly the dynamical evolution of the convective clouds and thus impacts stronger on the microphysical properties of the anvil. The presented results are under publication (Leroy et al, 2008).

2. MODEL DESCRIPTION AND SETUP

The 3D model with detailed (bin) microphysics used herein couples the 3D non-hydrostatic model of Clark and Hall (1991) with the Detailed Scavenging Model DESCAM (Flossmann et al., 1985) A detailed description of the microphysical package, including sensitivity studies of DESCAM under mixed phase conditions can be found in Leroy et al. (2007).

Below only a brief summary of the essential features is given. The microphysical model employs five distribution functions: three number density distributions functions respectively for the wet aerosol particles (AP), the drops and the ice crystals and two mass density distribution of aerosol particles inside drops and ice particles. The five functions are discretized over 39 bins that cover a range of radius from 1 nm to 6 µm for the wet AP and from 1 µm to 6 mm for the liquid or solid hydrometeors. All together, the detailed microphysics introduces 195 supplementary prognostic variables to the initial code.

The microphysical processes that are considered in the model are: condensational growth and activation/deactivation of AP, condensation and evaporation of droplets, coalescence, homogeneous and

heterogeneous nucleation, vapour deposition on ice crystals and riming. Droplet nucleation relies on the calculation of the activation radius derived from the Koehler equation (Pruppacher and Klett, 1997), but is also dependent on temperature as described in Leroy et al. (2007). Growth rate of drops and ice crystals are given by Pruppacher and Klett (1997). Homogeneous and heterogeneous nucleation follows respectively the works of Koop et al. (2000) and Meyers et al. (1992). Ice crystals are assumed to be spherical and the density of ice is 0.9 g m^{-3}. Coalescence and riming are treated with the numerical scheme of Bott (1998). The collection kernels for coalescence of drops are calculated with the collection efficiencies of Hall (1980) and the terminal velocities of Pruppacher and Klett (1997). Riming description includes collection of droplets by large ice crystals as well as collection of small ice particles by large drops. The collection kernels for riming are set to be the same as those for coalescence of drops, i.e. we assume that the collection efficiency of a spherical ice crystal is equal to the one of a water drop of the same mass.

Aggregation and secondary production of ice particles during riming is also neglected in the model for the moment.

To initialize the microphysics, aerosol particle spectra as a function of altitude are needed. In the first simulation aerosol particle spectra are almost identical to those used by Fridlind et al. (2004) in their case called “baseline” which combines aerosol measurements from the Twin Otter and Citation aircrafts on July the 18th and from the WB-57 on July the 19th. Aerosol particle spectra follow log-normal distributions. The total number of aerosol particles in the boundary layer is 1800 cm^{-3}. Aerosol particles are assumed to be ammonium sulphate, entirely soluble and with a molecular weight of 132 g mol^{-1}.

For the simulations presented in this paper, the model domain is 32 km x 32 km in the horizontal and 15 km in the vertical. The resolution is 250 m for both the horizontal and the vertical coordinates. The dynamical time step is 1 second. The thermodynamical conditions are given by the sounding from Miami airport at 15 UTC. To initialize convection, a perturbation (8 km wide and 2 km deep) is imposed in the north east part of the model domain and is maintained during the first ten minutes of integration in order to represent a localized sensible and latent heat flux. In the center of the perturbation the temperature is 1.5 °C higher and the relative humidity is 2 % higher than in the environment.

3. SIMULATION AND OBSERVATION

According to Heymsfield et al. (2005), the cloud reached the tropopause near 14 km altitude by the time of the aircraft penetration. The length of the in-cloud flight path can be estimated to 20 km with the knowledge of the aircraft speed (roughly 120 m s^{-1}) and the duration of the measurements (170 s).

In the simulations, a vigorous convective cell develops and exceeds rapidly 10 km height.

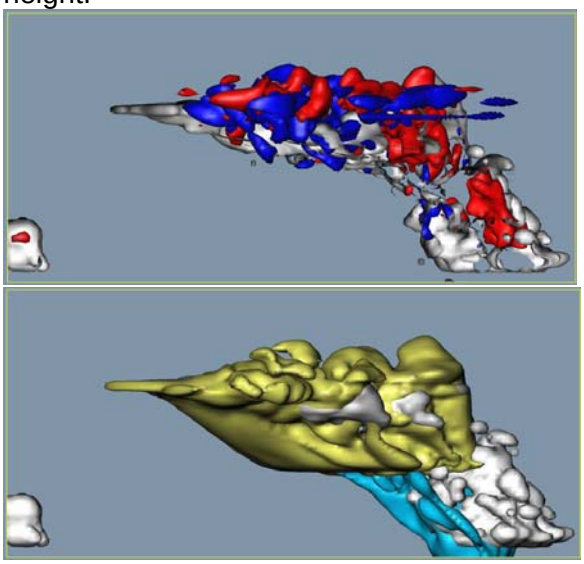

Fig.1: contours of the cloud after 42 min of integration; upper figure: the regions with updrafts larger than 8m/s in red and the downdrafts larger than 8m/s in blue; lower figure: the regions with cloud drops (grey), rain drops (blue) and ice crystals (yellow) larger than 0.01 g/m^3.

After 38 min of integration, cloud top is already above 12 km height. Through the

strong north-easterly wind in the high altitudes, the hydrometeors spread and an anvil forms.

Thus, after 42 minutes of integration (Fig.1), the anvil is roughly 20 km wide and the top of the cloud reaches in the simulation an altitude of 13 km. Therefore, the model results between 38 and 42 minutes of integration will be used to compare with the available airborne observations.

The principal measurements from the airplane are summarized in Table 1. Heymsfield et al. (2005) divided the flight track into four areas named A, B C and D. Letter A is attributed to the measurements in the anvil and is not discussed here. Regions B and C consider the updraft core of the cloud. Region B is entirely glaciated, vertical velocities reach 23 m s^{-1} and temperature increases to -33°C while the environment is about -35°C. On the contrary, vertical velocity stays below 13 m s^{-1} in region C. Liquid water is also detected in region C although temperature is 3°C lower than in region B (compare Fig. 4 in Heymsfield et al, 2005). Finally, region D refers to a downdraft area upwind of the core, with low water and ice content. In the following, we will keep this nomenclature.

Table 1 gives the observed and modeled values of the vertical velocity encountered along the simulated flight track from A to A'.

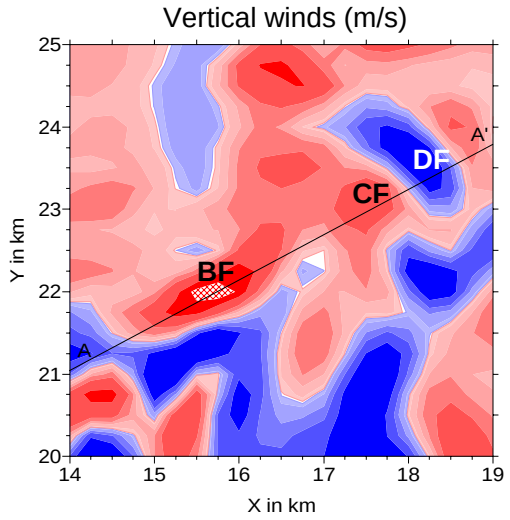

Fig.2: Simulated aircraft trajectory at z = 10.250 km at t = 41 min 40 s

The maximum vertical velocities are 25.5 m s^{-1} and 14 m s^{-1} respectively for regions B_F and C_F, and are in agreement with the corresponding measurements (23 m s^{-1} and 13 m s^{-1}). In the downdraft region, a value of -8 m s^{-1} was observed. In the model, the descent is slightly stronger with vertical velocities up to -13 m s^{-1}.

Heymsfield et al. (2005) presented size distributions measured with a FSSP probe for particles between 5 and 56 µm in diameter, and with a PMS 2D-C probe as well as a high volume particle spectrometer (HVPS) imaging probe for size ranges from about 60 µm to 6 cm. The IWC is then recalculated from those measurements. For the analysis of the FSSP probe, all particles were assumed to be solid spheres. For the presentation of the model results (cf. Table 1), the contribution of the small (r_i<40 µm) and the large ice particles (r_i>40 µm) to the IWC are also separated.

The measured IWC reaches 1 g m^{-3} in region B as well as in region C for both ice crystal categories. In our simulations, the IWC for precipitating ice is always larger than the IWC for cloud ice. In region B_F, the simulated values of IWC are clearly underestimated compared to the observations (respectively 0.2 and 0.7 g m^{-3} for cloud and precipitating ice). Agreement is much better in simulated region C_F with values of 0.75 and 1.2 g m^{-3} for cloud and precipitating ice. At least, the values of the IWC are low in both simulated and observed regions D. Upwind of downdraft region D cloud free conditions prevailed. In the model for this transition range some cloudy air still persist (IWC = 0.3 g m^{-3} ; LWC=0.2 g m^{-3}).

Liquid water was only observed in region C and the corresponding LWC was near 0.3 g m^{-3} which is well reproduced by DESCAM 3D: the LWC is negligible in region B_F and only reaches values of 0.3 g m^{-3} in region C_F (Tab.1).

According to Heymsfield et al. (2005), the measured number of particles along the flight path is 88 cm^{-3} in the glaciated region B but increases up to 221 cm^{-3} particles in region C where liquid water is present (Tab 1). However, it should be kept in mind that

reliable measurements of small ice crystals are difficult to obtain using FSSP devices (Gardiner and Hallett, 1985 ; Twohy et al., 1997).

At 10 km altitude, the maximum simulated numbers are close to 200 cm^{-3} for the drops and 5 cm^{-3} for the ice crystals in region C_F which is in agreement with the observations of Heymsfield et al. (2005). In region B_F, the simulated number of drops and ice crystals are both around 10 cm^{-3}. The total number of particles is thus underestimated compared to the observation of 88 cm^{-3} (Tab.1)

We can conclude that overall, the simulated parameters show quite good agreement with the observations. However, in region B, the simulated number of crystals is too low compared to the observations and this lack of ice particles leads to an underestimation of the IWC of both cloud and precipitating particles. The temperature variation along the AA' line differs from the observations but it is possible to improve the model results when shifting the flight path.

It has to be pointed out that the flight track is arbitrary in our simulation as the direction of the simulated anvil is different to the observed one at 10 km (compare satellite image in Heymsfield et al., 2005). This is due to a change in upper tropospheric wind direction between Miami and the measurement site. Thus, the flight track should have a different orientation with respect to the modeled cloud. As the regions B and C seem to correspond to different ascending areas, in the following, updrafts were identified where simulated vertical winds, temperature and microphysical parameters are all coherent with the observations, but the condition that these regions must be oriented along the prescribed south western flight track given in Heymsfield et al. (2005) will be disregarded. This will be called in the following 'virtual flight track'.

Table 2 shows the values of vertical velocity w, temperature T, LWC and IWC for two different regions along the virtual flight track.

Region	Parameter	Observed	Simulated
B	Maximum vertical velocity (m s^{-1})	23	25.5
	Maximum IWC for cloud ice (g m^{-3})	1.1	0.2
	Maximum IWC for precipitating ice (g m^{-3})	1.1	0.7
	Maximum number of hydrometeors (cm^{-3})	88	20
C	Maximum vertical velocity (m s^{-1})	13	14
	Maximum IWC for cloud ice (g m^{-3})	1	0.75
	Maximum IWC for precipitating ice (g m^{-3})	1.1	1.2
	Maximum LWC (g m^{-3})	0.3	0.3
	Maximum number of hydrometeors (cm^{-3})	221	205
D	Minimum vertical velocity (m s^{-1})	-8	-13
	Maximum IWC for cloud ice (g m^{-3})	0.4	0.2
	Maximum IWC for precipitating ice (g m^{-3})	0.4	0.45
	Maximum number of hydrometeors (cm^{-3})	20	10

Table 1 : Observed (taken from Heymsfield et al, 2005) and simulated values of vertical velocity, liquid and ice water content along the flight track AA'.

	Position		**Vertical wind**	**Temperature**	**LWC**	**IWC**
region	X (km)	Y (km)	(m s^{-1})	(°C)	(g m^{-3})	(g m^{-3})
B_v	20.75	24.25	16.2	-34.5	0.1	1.7
C_v	19	26	9.6	-36.8	0.5	1.0

Table 2 : Vertical velocity, temperature, LWC and IWC for two regions along the virtual flight track in the model domain after 38 min 20 s of integration corresponding to the observational feature of regions B and C presented in Table 1.

The altitude of 10.125 km is the same for the two regions: The initial sounding gives a temperature of -36 °C for this altitude. The parameters at B_v (*v* for virtual) are close to the observations in region B: the vertical wind is 16.2 m s^{-1}, temperature is 1.5 °C higher than the environmental value, and liquid water is almost negligible. At position C_v the vertical winds are around 10 m s^{-1}, the temperature of -36.8 °C is lower than the environment, and liquid water and ice are both present. In fact, between 35 and 41 minutes of integration, it is possible to find several regions that are close to 10 km in altitude and that match the observations either for the region B or C. Here we focused on these two points because they appeared at the same time: 38 min 20 s. Regarding the position of the two regions in the model domain, our region C_v is north-west from region B_v, 2.6 km apart, which is coherent with the observations.

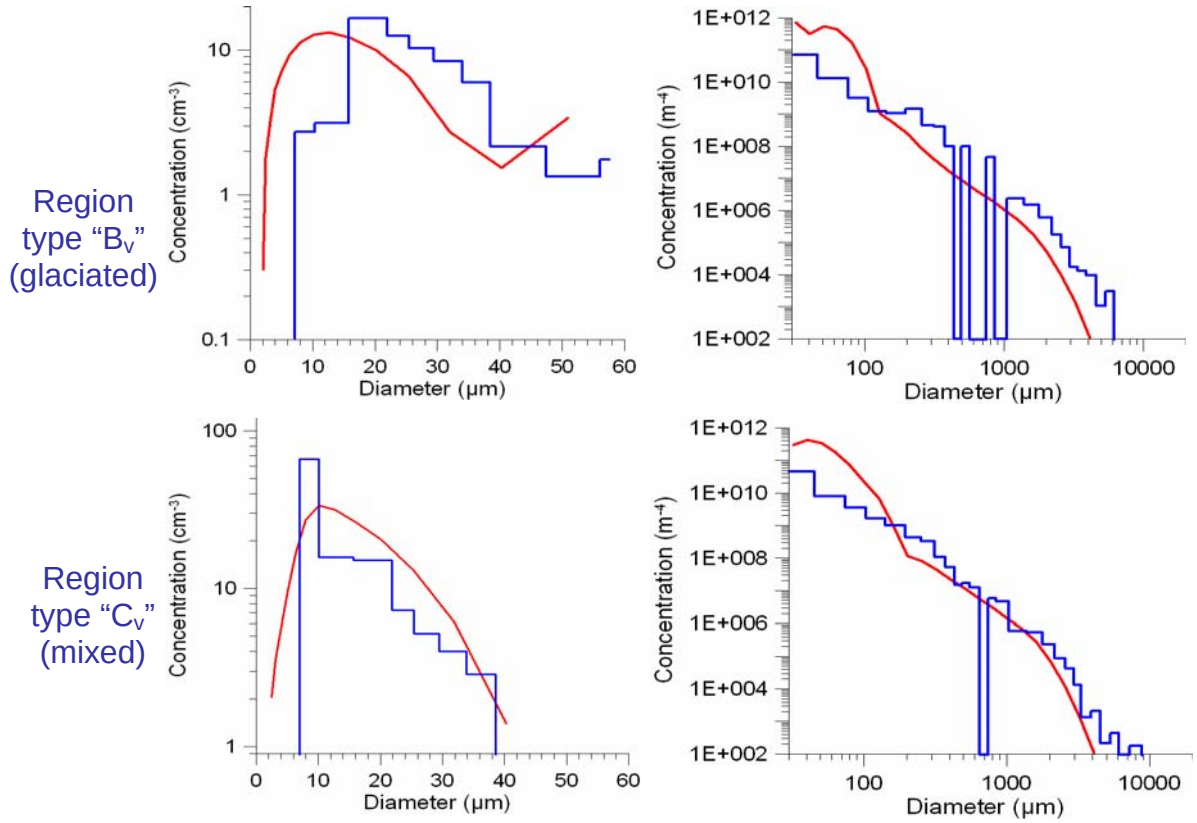

Fig.3: Modelled particle spectra in red for position B_V and C_V (Tab 2) compared to the observed histograms by Heymsfield et al. (2005) in blue.

Fig. 3 compares simulated and observed particle spectra in region B (position [6] in Heymsfield et al., 2005) and C (position [8]). Model results agree quite well with observations in region B and C (Figs. 3). Simulated particle spectra and integrated values are consistent with measurements for both small and large sizes.

Thus, we can conclude that generally the model succeeds in reproducing the observations.

4 IMPACT OF BOUNDARY LAYER AEROSOL PARTICLES

Following Fridlind et al. (2004), we then investigated the role of the aerosol particles above 6 km height on the development of the cloud (anvil). In a numerical experiment,

the number of aerosol particles was reduced to only 5% of the number in the reference case for all layers above 6 km. We did not follow Fridlind et al. (2004) who reduced the AP number concentration to 0 as our model does not allow droplet formation by homogeneous nucleation. The total number of aerosol particles is now 150 cm^{-3} instead of 3000 cm^{-3} for the reference case between 6 and 10 km, and 5 cm^{-3} instead of 100 cm^{-3} above 10 km. This second calculation will be referred to as case "5%AP6".

In the model, the aerosol particles serve both as cloud condensation nuclei and ice nuclei. Thus, changes in the aerosol particles concentration are potentially able to impact on droplet activation as well as homogeneous and heterogeneous nucleation. However, as mentioned before, heterogeneous nucleation is described by the Meyers et al. (1992) formula which relates the number of ice nuclei only to supersaturation. Thus, changes in the aerosol concentration can only have an indirect impact on heterogeneous nucleation by changing the supersaturation.

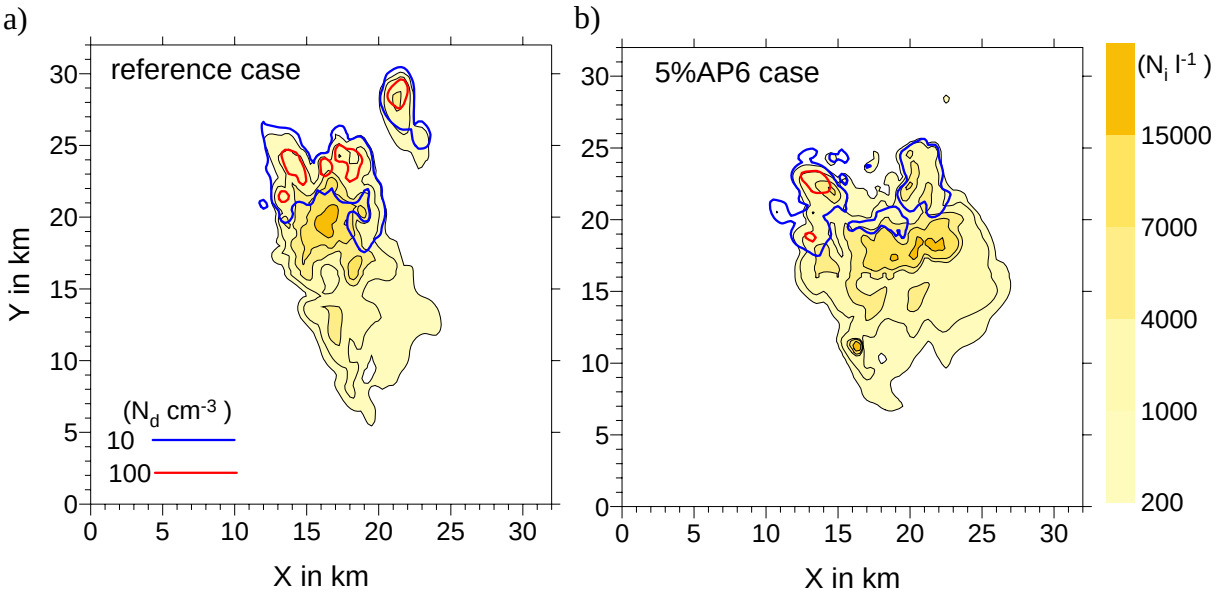

Figure 4 : Number concentration of ice crystals (l^{-1}) in yellow and droplets (cm^{-3}, blue and red lines) at 10 km and after 42 minutes of integration for the reference (Fig. 3a) and the 5%AP6 (Fig. 3b) cases.

Figs. 4a and b display the horizontal extension of these simulated clouds in 10 km altitude after 42 minutes of integration. Fig. 4a depicts the results for the reference case, Fig. 4b the results for the 5%AP6 case. Both figures display the number concentrations of ice crystals and cloud droplets and both cases show numerous similarities: the number concentrations for the ice crystals cover the same order of magnitude between 200 to 15000 particles /l, the number of cloud droplet is significantly larger but their presence is restricted to small regions located at the upwind edge of the cloud field associated to the updraft core. Furthermore the maxima in crystal numbers are located downwind from those of the drop numbers in both cases.

Although the size of the horizontal areas of both the droplet field and the crystal field do not differ significantly between the reference and the 5%AP6 case, the shape shows several differences. In the reference case the ice crystal field is mainly oriented from north to south while the horizontal distribution of the crystals in the 5%AP6

case indicates no privileged direction but extends also to the east and the west. The main surface area occupied by the droplets in the reference case appears in a connected and almost closed field, the droplet field for the 5%AP6 case, however, is divided in several smaller patches.
Considering also the evolution of the other cloud properties not shown here this last finding suggests that in the case with negligible AP concentration above 6 km the cloud is more advanced in its time evolution and the central convective core starts to decay. We can conclude from this comparison that both cases have experienced different dynamical evolutions.
However, our modeling results cannot confirm the hypothesis of Fridlind et al. (2004) that mid-tropospheric AP are regulating the ice crystal concentration in the studied sub-tropical anvil. The dominating hydrometeors in the anvil are ice crystals and their number does not show an important variation when the AP number concentrations are modified between 6-10 km. As we cannot confirm the role of the mid-tropospheric aerosol, we will study in the following the role of the boundary layer aerosol.

5 IMPACT OF BOUNDARY LAYER AEROSOL PARTICLES

As already shown by Yin et al. (2005), aerosol particles from the boundary layer can be transported up to the high levels, detrained and then re-entrained at mid-cloud levels. Moreover, Heymsfield et al. (2005) used a Paluch diagram (Paluch, 1979) to analyze the role of entrainment for their observations and found that the air they sampled at 10 km height seems to be a mixture of cloud base air and air that originated about 2 km above aircraft level. Thus, it seems highly possible that aerosol particles from the boundary layer impact on the anvil properties.
For this study we use again the same aerosol spectra as Fridlind et al. (2004). In the so-called *clean* case, the number of aerosol particles below 1 km is reduced to 400 cm^{-3} instead of 1800 cm^{-3} in the reference case. In addition, for the *polluted* boundary layer, this number is increased up to 6500 cm^{-3}. Above 1 km, the aerosol particle spectra remain identical to the reference case.

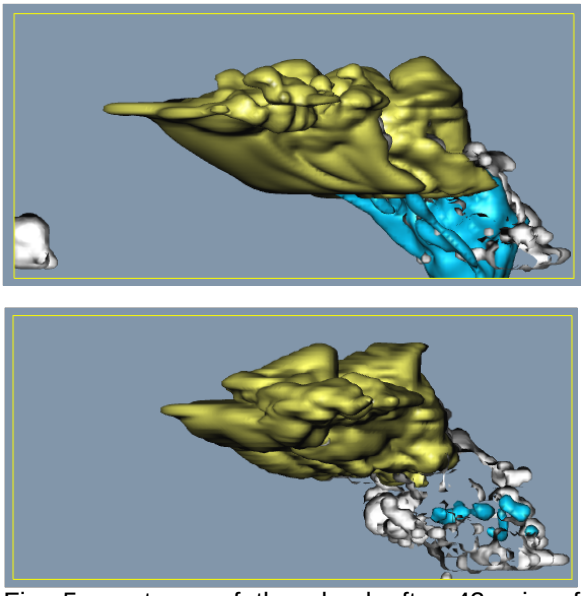

Fig. 5: contours of the cloud after 42 min of integration; upper figure (a): clean case; lower figure (b): polluted case; with cloud drops (grey), rain drops (blue) and ice crystals (yellow) larger than 0.01 g/m^3.

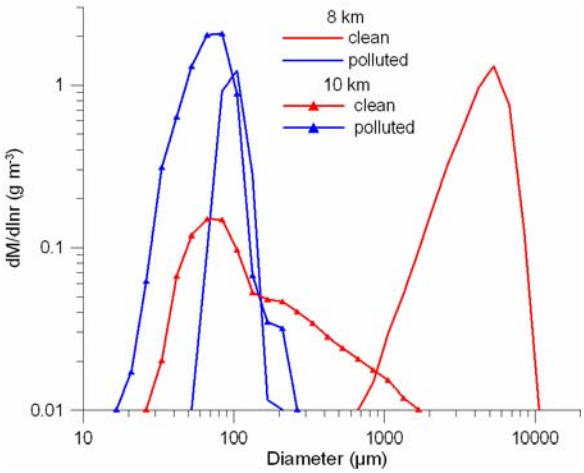

Fig.6: Modelled mean mass spectra of ice crystals at 8 and 10 km height and after 38 min of integration for both polluted and clean cases.

The horizontal and vertical distribution of cloud ice and precipitating ice water content is shown in Fig 5. Fig. 5 demonstrates that the larger anvil for the clean cloud in 10 km is composed of ice crystals. The horizontal

extension of cloud top and anvil in the polluted case (Fig. 5b) is significantly smaller, but the cloud ice content is higher and thus indicates a stronger number concentration of small ice crystals. The content of precipitating ice covers the same order of magnitude with maximum values of more than 1 g/m^3 in both cases. The numerical results for the precipitating ice (not shown here) are strongly determined by the cut-off radius chosen to split the ice crystal spectrum in cloud and precipitating particles. In our calculation a cut-off radius of 40 µm was used. Fig. 6 presents the mean mass distribution function of the ice crystals at 8 and 10 km altitude. We can detect from this illustration that the small mode of the ice spectra also counts for the precipitating ice as its diameter exceeds 80 µm. Thus the high content of precipitating ice for the polluted case is caused by these medium sizes of the ice crystals in the upper tropospheric levels.

In the polluted case, the size of the ice crystals never exceeds 300 µm in diameter at 8 as well as at 10 km height. In the clean case, the IWC is low at 10 km at 38 min with only very few ice crystals with diameters above 300 µm. On the contrary, at 8 km, the ice spectrum in the clean case covers now precipitating diameters from 1 mm to 1 cm (Fig.6).

From this numerical analysis, it is evident that the aerosol loading in the boundary layer has important consequences on the microphysical properties of deep convective clouds even at altitudes as high as 10 km. The number of aerosol particles determines primarily the mass of precipitating hydrometeors and therefore, impacts on the dynamics and thus on cloud development. As the dynamical evolution of the cloud is strongly influenced by the number of AP originating from the boundary layer, changes in the lowest layers of the cloud can easily propagate to the highest altitude. These findings are e.g. in agreement with those of Carrió et al. (2007) who extended the work of van den Heever et al. (2006) to the anvil properties and showed that the enhancement of CCN effects on ice crystals spectra in the anvil-cirrus cloud.

6 CONCLUSIONS

In this study a high resolved 3D cloud model with detailed microphysics called DESCAM 3D is used to simulate a deep convective cloud with anvil. The studied cloud was observed during the CRYSTAL-FACE campaign and is described in Heymsfield et al (2005). Measurements of vertical velocity and temperature as well as microphysical parameters (LWC, IWC, hydrometeors spectra) are available for both the anvil and the updraft core of the cloud at 10 km height. The updraft core is divided into two regions: one is entirely glaciated, vertical winds are up to 20 m s^{-1} but the temperature of -33°C is about 1.5°C higher than the environment, the other region is colder than the environment, vertical velocity is around 10 m s^{-1} and high numbers of small water droplets are present.

The model is able to simulate realistically the cloud with a top up to 14 km and a large anvil. Simulated flight trajectories at 10 km show good agreement with the observations for the vertical winds and the microphysical parameters. In particular, the simulated spectra are generally consistent with those measured, although improvements in the results may be obtained from further model improvements. This concerns e.g. a decreasing value of the ice density with increasing ice crystal size as well as a consideration of ice habits. Furthermore, a higher vertical and horizontal resolution down to a few meters would be desirable to resolve small scale supersaturation peaks.

Following the work of Fridlind et al (2004), we then investigated the respective role of mid-tropospheric and boundary layer aerosol particles on cloud properties. Our findings significantly differ from those of Fridlind et al (2004) who concluded from their modeling studies that aerosol entrained between 6 and 10 km account for about two-thirds of the anvil nuclei. We found that aerosol particles above 6 km have only a limited impact on the number of small cloud droplets prevailing in or next to

the updraft cores at 10 km but do not change the number of ice crystals in the dominating anvil regions. On the other hand we could identify changes in the dynamical evolution of the cloud which are caused by changes in thermodynamic properties (especially supersaturation). Theses dynamical and thermodynamical differences suggest that a comparison between simulations under low number concentrations and regular conditions do not allow to correctly quantify the role of mid-tropospheric aerosols on cloud formation in upper tropospheric levels.
Modifications in the dynamical and microphysical evolution of the cloud are even more pronounced when changing from a clean to a polluted boundary layer. In clean air masses, rain drops formed in large quantities early in cloud development. Those big drops fall through the cloud updraft and hamper cloud development. On the contrary, clouds forming in a polluted environment are characterized by a huge number of small cloud droplets and rain formation is suppressed. Updrafts in the polluted cloud extend rapidly to high altitudes and thus, the polluted cloud reaches higher levels. Our results agree with those of Khain et al. (2005) who investigated the aerosol impact on the dynamics of deep convective clouds with a 2D model with spectral microphysics. However, concerning the case studied it is evident that a 3D dynamical model is mandatory in order to reproduce the complex dynamics.

7 ACKNOWLEDGEMENTS

The calculations for this paper have been done on computer facilities of the “Institut du Développement et des Ressources en Informatique Scientifique” (IDRIS, CNRS) in Orsay (France) and the “Centre Informatique National de l’Enseignement Supérieur” (CINES) in Montpellier (France), under project no.940180. The authors acknowledge with gratitude the hours of computer time and the support provided.

8 REFERENCES

Bott A., 1998 : A flux method for the numerical solution of the stochastic collection equation. *J. Atmos. Sci.*, **55**, 2284-2293.

Carrió, G. G., S. C. van den Heever and W. R. Cotton, 2007 : Impacts of nucleating aerosol on anvil-cirrus clouds : A modeling study. *Atmos. Res.*, **84**, 111-131.

Clark T. L., and W. D. Hall, 1991 : Multi-domain simulations of the time dependent Navier-Stokes equations : benchmark error analysis of some nesting procedure, *J. Comp. Phys.*, **92**, 456-481.

Flossmann A. I., W. D. Hall and H. R. Pruppacher, 1985 : A theoretical study of the wet removal of atmospheric pollutants. Part I : The redistribution of aerosol particles captured through nucleation and impaction scavenging by growing cloud drops. *J. Atmos. Sci.*, **42**, 583-606.

Fridlind A. M., A. S. Ackerman, E. J. Jensen, A. J. Heymsfield, M. R. Poellot, D. E. Stevens, D. Wang, L. M. Miloshevich, D. Baumgardner, R. P. Lawson, J. C. Wilson, R. C. Flagan, J. H. Seinfeld, H. H. Jonsson, T. M. VanReken, V. Varutbangkul and T. A. Rissman, 2004 : Evidence for the predominance of mid-tropospheric aerosols as subtropical anvil cloud nuclei. *Science*, **304**, 718-721.

Gardiner B. A. and J. Hallett, 1985 : Degradation of in-cloud forward scattering spectrometer probe measurements in the presence of ice particles. *J. Atmos. Oceanic. Technol.*, **2**, 171-180.

Hall W. D., 1980 : A detailed microphysical model within a two-dimensional dynamic framework : Model description and preliminary results. *J. Atmos. Sci.*, **37**, 2486-2506.

Heymsfield A. J., L. M. Miloshevich, C. Schmitt, a. Bansemer, C. Twohy, M. R. Poellot, A. Fridlind and H. Gerber, 2005 : Homogeneous ice nucleation in subtropical and tropical convection and its influence on cirrus anvil microphysics. *J. Atmos. Sci.*, **62**, 41-64.

Khain A. P., D. Rosenfeld and A. Pokrovsky, 2005 : Aerosol impact on the dynamics and microphysics of deep convective clouds. *Q. J. R.*

Meteorol. Soc., **131**, 2639-2663. DOI:10.1256/qj.04.62

Koop T., H. P. Ng, B. Luo, A. Tsias and T. Peter, 2000 : Water activity as the determinant for homogeneous ice nucleation in aqueous solutions. *Nature*, **406**, 611-615.

Leroy D., W. Wobrock, A. I. Flossmann, 2008: The role of boundary layer aerosol particles for the development of deep convective clouds: a high-resolution 3D model with detailed (bin) microphysics applied to CRYSTAL-FACE *Atmos. Res.*, under revision.

Leroy D., W. Wobrock, and A. I. Flossmann, 2007 : On the influence of the treatment of aerosol particles in different bin microphysical models : a comparison between two different schemes. *Atmos. Res.*, **85**, 269-287. doi : 10.1016/j.atmosres.2007.01.003

Meyers M. P., P. J. Demott and W. R. Cotton, 1992 : New primary ice nucleation parameterizations in an explicit cloud model. *J. Appl. Met.*, **31**, 708-721.

Paluch I. R., 1979 : The entrainment mechanism in Colorado cumuli. *J. Atmos. Sci.*, **36**, 2467-2478.

Pruppacher H. R. and J.D. Klett, 1997 : *Microphysics of clouds and precipitation*. 2nd ed. Kluwer Academic, 954p.

Twohy C. H., A. J. Schanot and W. A. Cooper, 1997 : Measurements of condensed water content in liquid and ice clouds using an airborne counterflow virtual impactor. *J. Atmos. Oceanic. Technol.*, **14**, 197-202.

van den Heever S. C., G. G. Carrió, W. R. Cotton, P. J. DeMott and A. J. Prenni, 2006 : Impacts of nucleating aerosol on Florida storms. Part I : Mesoscale simulations. *J. Atmos. Sci.*, **63**, 1752-1775.

Yin Y., K. S. Carslaw and G. Feingold, 2005 : Vertical transport ad processing of aerosols in a mixed-phase convective cloud and the feedback on cloud development. *Q. J. R. Meteorol. Soc.*, **131**, 221-245.